



# City Research Online

## City St George's, University of London

**Citation:** Wei, Z., Yang, B., You, Q., Tsavdaridis, K. D. & Jia, S. (2025). Study on multi-parameter optimization of seismic isolation bearings for continuous girder bridges considering interactions among key parameters. *Scientific Reports*, 15(1), 18448. doi: 10.1038/s41598-025-02155-z

This is the published version of the paper.

This version of the publication may differ from the final published version. To cite this item please consult the publisher's version.

**Permanent repository link:** <https://openaccess.city.ac.uk/id/eprint/35311/>

**Link to published version:** <https://doi.org/10.1038/s41598-025-02155-z>

**Copyright and Reuse:** Copyright and Moral Rights remain with the author(s) and/or copyright holders. Copies of full items can be used for personal research or study, educational, or not-for-profit purposes without prior permission or charge, unless otherwise indicated, provided that the authors, title and full bibliographic details are credited, a hyperlink and/or URL is given for the original metadata page and the content is not changed in any way. For full details of reuse please refer to [City Research Online policy](#).



# OPEN Study on multi-parameter optimization of seismic isolation bearings for continuous girder bridges considering interactions among key parameters

Zhaolan Wei<sup>1,2✉</sup>, Bowen Yang<sup>1</sup>, Qixuan You<sup>1</sup>, Konstantinos Daniel Tsavdaridis<sup>2</sup> & Shaomin Jia<sup>1</sup>

Traditional isolation design for continuous girder bridges often focuses on single-parameter tuning, overlooking the complex interactions among yield strength, pre-yield stiffness, and post-yield stiffness. This paper proposes a multi-parameter optimization method to systematically investigate the nonlinear influence of each parameter on the seismic performance of bridges. First, using a conventional particle swarm optimization (PSO) algorithm, the individual and combined effects of each parameter on key response indicators are identified. On this basis, an adaptive particle swarm optimization (APSO) algorithm with dynamic inertia weights and learning factors is introduced to broaden the search space, expedite convergence, and reduce the likelihood of becoming trapped in local optima. Numerical studies indicate that, compared with the standard PSO method, APSO can reduce the total number of iterations by up to 40% while maintaining solution accuracy. The underlying mechanism is that APSO preserves particle diversity and dynamically adjusts the balance between global and local searches, thereby rapidly identifying the optimal bearing configuration. Compared with single-parameter or orthogonal design methods, the APSO-based multi-parameter optimization strategy significantly enhances structural ductility, as reflected by notable reductions in pier-top displacement and pier-bottom shear force. These findings underscore the robustness and efficiency of APSO in designing isolation bearings for high-dimensional problem spaces.

Major earthquakes, such as the 1995 Hanshin-Awaji Earthquake in Japan and the 2008 Wenchuan Earthquake in China, have repeatedly underscored the significant vulnerability of bridges during large-scale seismic events<sup>1</sup>. For bridge structures located in areas of intense seismic activity, the failure of any component can lead to immense economic losses and severely disrupt post-disaster rescue and reconstruction efforts. In response, seismic isolation technology has gained increasing prominence in bridge engineering, as it effectively decouples the superstructure from seismic motions and thus mitigates structural damage. Among these technologies, isolation bearings play a pivotal role in dissipating seismic energy; their performance is crucial for ensuring bridge safety and functionality under strong earthquakes<sup>2</sup>. In areas prone to high-intensity seismic activity, the careful selection of optimal bearing parameters can markedly improve the reliability and serviceability of continuous girder bridges, thereby securing lifeline transportation networks and facilitating rapid emergency response operations.

Although existing research has made notable strides in elucidating the nonlinear behavior of isolation bearings, most work has focused on individual parameters, such as bearing yield strength or stiffness<sup>3</sup>. Amiri et al.<sup>4</sup> studied the seismic response of triple friction pendulum isolators under near-fault ground motions, identifying through detailed sensitivity analysis the optimal bearing parameters that significantly improve overall damping efficiency. Peng et al.<sup>5</sup> proposed a reliability-based optimization framework for adaptive sliding isolation systems, incorporating sensitivity analysis and magnetically sliding bearings to enhance seismic performance. Zhong et al.<sup>6</sup> developed a risk-driven sensitivity analysis and optimization procedure based on Gaussian process surrogate models, effectively lowering seismic risk through refined bearing parameter selection. Concurrently, Gur et al.<sup>7</sup>

<sup>1</sup>School of Civil Engineering, Sichuan Agricultural University, Chengdu 611830, China. <sup>2</sup>Department of Engineering, School of Science & Technology, City University of London, Northampton Square, London EC1V 0HB, UK. ✉email: wzhlana@sicau.edu.cn

focused on the stochastic optimization of shape memory alloy rubber bearings, showing that such bearings can markedly boost isolation capacity under random seismic scenarios. While these single-parameter approaches deepen our understanding of isolation performance, they often prove inadequate for practical engineering applications, especially when multiple parameters interact to shape the overall seismic response. For continuous girder bridges with significant variations in pier heights, curvature effects, or other complex factors, relying solely on single-parameter analyses risks overlooking critical coupling effects among bearing design variables. Consequently, examining bearing design from a multi-parameter perspective not only aligns better with real-world conditions but also offers a more comprehensive strategy for enhancing seismic safety.

To address the challenges inherent in multi-parameter design, researchers have increasingly adopted computational intelligence methods—particularly PSO—to systematically identify optimal isolation bearing parameters. For instance, Pang et al.<sup>8</sup> formulated a risk-based design and optimization framework for shape memory alloy-restrained sliding bearings in highway bridges subjected to near-fault seismic loading, employing PSO to reduce seismic risk. Xia et al.<sup>9</sup> introduced an improved PSO technique for structural model updating in high-dimensional bridge systems, achieving higher accuracy and efficiency using ambient vibration data. Tran-Ngoc et al.<sup>10</sup> devised a hybrid model updating approach for multi-span railway bridges, combining orthogonal diagonalization with an enhanced PSO algorithm to lower computational complexity. Chen et al.<sup>11</sup> proposed an improved PSO-based analysis method for the construction stages of suspension bridges, integrating the standard PSO with genetic algorithms to obtain a more precise system configuration. Li et al.<sup>12</sup> adopted a novel PSO algorithm to develop an optimal sensor placement strategy for long-span cable-stayed bridges, reducing costs while enhancing measurement efficiency. Quaranta et al.<sup>13</sup> employed differential evolution and PSO to identify key parameters of isolation devices, confirming the feasibility of nontraditional techniques in isolator characterization. Zhang et al.<sup>14</sup> used PSO for simultaneous inversion of pre-stack seismic data, improving elastic parameter models and bolstering both the precision and reliability of geophysical interpretations. Similarly, recent machine learning approaches, such as Wei et al.<sup>15</sup>, employed extensive datasets to predict seismic responses and fragility of high-speed railway bridges, showcasing strengths in predictive efficiency but reliance on data availability. Additionally, Wei et al.<sup>16</sup> introduced novel ductile piers with improved deformation capabilities under seismic loads, potentially influencing the performance requirements and optimization of isolation bearings. While various state-of-the-art optimization algorithms such as Differential Evolution (DE), Genetic Algorithm (GA), Grey Wolf Optimizer (GWO), and Ant Colony Optimization (ACO) have demonstrated success in structural optimization tasks, PSO remains particularly well-suited for multi-parameter problems characterized by continuous search spaces, nonlinearity, and complex constraint interactions. PSO has demonstrated consistent robustness and efficiency specifically in engineering design optimization problems characterized by nonlinear, multi-modal, and high-dimensional search spaces, typical of seismic isolation bearing optimization scenarios. Compared to DE and GA, PSO typically requires fewer control parameters and exhibits faster convergence in scenarios involving moderate noise or multimodal objective functions. Moreover, hybrid PSO variants have been shown to outperform other algorithms in computational efficiency and robustness when applied to civil engineering optimization tasks. Given the high-dimensional, nonlinear, and computationally intensive nature of seismic isolation bearing design, PSO—especially in its enhanced, adaptive forms—presents a compelling choice. The present study builds on this foundation by integrating adaptive strategies into the PSO framework, specifically tailored to the physical constraints and seismic demands of continuous girder bridges. Despite these advances, conventional PSO still faces challenges in balancing convergence speed and robustness in design spaces with higher dimensionality and multiple constraints. To tackle this issue, the present study introduces an improved particle swarm optimization (APSO) that adaptively adjusts inertia weights and learning factors, thereby enhancing both optimization efficiency and convergence speed. This improvement is especially advantageous for large-scale, nonlinear isolation design problems, where computational efficiency is of paramount importance.

The primary novelty of this work lies in integrating multi-parameter isolation design with an enhanced particle swarm algorithm specifically tailored for continuous girder bridges, thus forming a systematic approach. By comprehensively considering critical nonlinear bearing characteristics under bidirectional seismic excitation—namely yield strength, pre-yield stiffness, and post-yield stiffness—our study transcends the limitations of single-parameter optimization. Moreover, we demonstrate that APSO not only accelerates convergence but also improves the optimal isolation performance, making it more effective than conventional PSO or other common optimization strategies under the complex conditions typical of continuous girder bridges. In Sect. 2, we derive the particle swarm formulation for the multi-parameter optimization of damping-isolation bearings, while in Sect. 3 we enhance the traditional PSO, proposing an adaptive particle swarm algorithm. In Sect. 4, comparative experiments against conventional optimization methods illustrate APSO's superior performance in multi-parameter isolation bearing design, offering theoretical insights and practical guidance for seismic bridge design.

### Optimization of damping-isolation bearings using particle swarm optimization

In the design of continuous girder bridges located in high-intensity seismic zones, isolation bearing parameters play a pivotal role in determining the overall seismic performance of the structure. Conventional optimization approaches often concentrate on a single parameter (e.g., yield strength or stiffness) to reduce design complexity; however, such simplifications tend to overlook the interactions among multiple bearing parameters under realistic seismic demands. Conversely, multi-parameter optimization provides a holistic understanding of bearing responses under severe seismic excitations, thereby markedly enhancing the resilience of critical transportation infrastructure<sup>17</sup>.

This section introduces the PSO algorithm and discusses its application in multi-parameter bearing optimization. Compared with conventional methods, PSO offers strong global search capabilities and high

computational efficiency, making it particularly suitable for large-scale structural problems involving nonlinear material behavior and multi-degree-of-freedom systems.

PSO is a classic intelligent optimization method. It typically uses a random strategy to initialize multiple candidate solutions (particles) and then iteratively updates these solutions according to a prescribed procedure until an optimal solution is found based on a certain fitness criterion. At each iteration, particles are adjusted according to two “extreme” values within the swarm: the first is the historical best solution found by the particle itself, denoted as  $pBest$ ; the second is the historical best solution found by the entire population, denoted as  $gBest$ <sup>18,19</sup>.

The iterative process through which each particle seeks the optimal solution can be described mathematically by Eqs. (1) and (2)<sup>20</sup>. In an  $n$ -dimensional target search space, the position and velocity of the  $d$ -th particle can be expressed as:

$$X_i = \{x_{i1}, x_{i2} \cdots, x_{in}\}, i = 1, 2, \cdots, n \quad (1)$$

$$V_i = \{v_{i1}, v_{i2} \cdots, v_{in}\}, i = 1, 2, \cdots, n \quad (2)$$

During iterative optimization, the  $pBest$  and  $gBest$  of the  $i$ -th particle at the current time, as well as their corresponding particle position vectors, can be represented by:

$$pBest_i = \{pBest_{i1}, pBest_{i2} \cdots, pBest_{in}\}, i = 1, 2, \cdots, n \quad (3)$$

$$gBest_i = \{gBest_{i1}, gBest_{i2} \cdots, gBest_{in}\}, i = 1, 2, \cdots, n \quad (4)$$

$$\vec{P}_i = \{p_{i1}, p_{i2} \cdots, p_{in}\}, i = 1, 2, \cdots, n \quad (5)$$

$$\vec{G}_i = \{g_{i1}, g_{i2} \cdots, g_{in}\}, i = 1, 2, \cdots, n \quad (6)$$

Throughout the iterative procedure, all particles in the swarm strictly search within a prescribed region, denoted by  $\{R = D | D = (e_1, e_2, \cdots, e_d), -X_d^{\max} \leq e_d \leq X_d^{\max}, d = 1, 2, \cdots, D\}$ . The maximum search range and maximum search speed for each particle are represented by  $X^{\max} = \{x_1^{\max}, x_2^{\max}, \cdots, x_i^{\max}\}$  and  $V^{\max} = \{v_1^{\max}, v_2^{\max}, \cdots, v_i^{\max}\}$ , respectively. When  $x_i > X_i^{\max}, v_i > V_i^{\max}$ , set  $x_i = X_i^{\max}, v_i = V_i^{\max}$ ; and when  $x_i < -X_i^{\max}, v_i < -V_i^{\max}$ , set  $x_i = -X_i^{\max}, v_i = -V_i^{\max}$ .

Particle positions are updated by  $x_{id}^{t+1} = x_{id}^t + v_{id}^{t+1}$ , following the iterative procedure outlined below:

- (1) Initialize particle positions and velocities, setting initial solutions as each particle's individual best ( $pBest_i$ ) positions and selecting the overall best as the global best ( $gBest_i$ ).
- (2) Calculate each particle's objective function (fitness).
- (3) Update each  $pBest_i$  if its current fitness is superior; similarly, update the  $gBest_i$  if a new global optimum is identified.
- (4) Update the  $d$ th-dimensional position and velocity for each particle  $i$ .
- (5) Check whether the current solution satisfies the termination condition; if it does, output  $gBest$  and terminate. Otherwise, return to step (2) and continue iterating until the termination condition is met.

In PSO, one of the most critical factors is the velocity update scheme, which plays a decisive role in both optimization performance and convergence speed. Typically, three commonly used formulas are adopted for velocity updating, as given in Eqs. (7), (9), and (11), with the corresponding position-update formulas provided in Eqs. (8), (10), and (12).

$$v_{id}^{t+1} = v_{id}^t + c_1 r_1 (pBest_{id}^t - x_{id}^t) + c_2 r_2 (gBest_{id}^t - x_{id}^t) \quad (7)$$

$$x_{id}^{t+1} = x_{id}^t + v_{id}^{t+1} \quad (8)$$

where  $i = 1, 2, \cdots, n$  represents the individual particles, and  $n$  is the total number of particles;  $v_{id}^{t+1}$  is the  $d$ -dimensional velocity of the  $i$ -th particle at iteration  $t + 1$ ;  $v_{id}^t$  is the  $d$ -dimensional velocity of the  $i$ -th particle at iteration  $t$ ;  $c_1, c_2$  are the learning factors for the  $pBest$  and  $gBest$ , also known as acceleration constants, typically set to  $c_1 = c_2 = 2$ ;  $r_1, r_2$  are uniform random numbers within the range (0, 1), which adjust the  $pBest$  and  $gBest$  to enhance the diversity of the swarm;  $x_{id}^{t+1}$  is the position of the particle after  $t + 1$  iterations; and  $x_{id}^t$  is the position of the particle after  $t$  iterations.

$$v_{id}^{t+1} = \theta v_{id}^t + c_1 r_1 (pBest_{id}^t - x_{id}^t) + c_2 r_2 (gBest_{id}^t - x_{id}^t) \quad (9)$$

$$x_{id}^{t+1} = x_{id}^t + v_{id}^{t+1} \quad (10)$$

where  $\theta$  is the constraint factor, which is a constant coefficient in front of the velocity when the position is updated.

$$v_{id}^{t+1} = \omega v_{id}^t + c_1 r_1 (pBest_{id}^t - x_{id}^t) + c_2 r_2 (gBest_{id}^t - x_{id}^t) \quad (11)$$

$$x_{id}^{t+1} = x_{id}^t + v_{id}^{t+1} \quad (12)$$

where  $\omega$  is referred to as the inertia factor, and its value is non-negative. In typical iterative optimization processes,  $\omega$  is usually a dynamic value. It is generally more effective for optimization compared to a fixed value. The value of  $\omega$  typically changes linearly, with the most commonly used strategy being the linear decreasing weight (LDW) strategy:  $\omega^{(t)} = (\omega_{ini} - \omega_{end}) (G_k - g) / G_k + \omega_{end}$ , where  $G_k$  represents the maximum number of iterations,  $\omega_{ini}$  is the initial inertia weight, and  $\omega_{end}$  is the inertia weight at the maximum iteration. A typical choice for inertia weights is  $\omega_{ini} = 0.9$  and  $\omega_{end} = 0.4$ . When the inertia weight is large, the global optimization ability is stronger, but the local optimization ability is weaker. When the inertia weight is small, the global optimization ability is weaker, but the local optimization ability is stronger.

The polynomial formula consists of three terms:

- (1) Inertia term: Retains particle velocity from the previous iteration, acting as a momentum to explore solution space.
- (2) Self-cognitive term: Guides particles based on their own best-known position, reflecting individual experience and promoting local search efficiency.
- (3) Social-cognitive term: Directs particles toward the global best-known solution, leveraging collective swarm experience to enhance convergence toward the global optimum.

These components collectively influence both convergence speed and optimization performance, and standard velocity updating equations referenced in the manuscript are employed.

Equations (7) and (9) are generally regarded as the standard forms of PSO.

In summary, the basic principles of the particle swarm algorithm can be represented by the flowchart shown in Fig. 1.

The PSO algorithm has opened new research and practical pathways in the field of seismic design for bridges. In the face of complex engineering challenges such as large-span bridges, traditional design methods often struggle to provide comprehensive and convenient solutions, especially when dealing with parameter optimization. Known for its flexibility and efficiency, the PSO algorithm is particularly suitable for solving multi-parameter optimization problems. By simulating the search behavior of particles within the parameter space, the PSO algorithm can explore a wide design space and comprehensively optimize the three nonlinear characteristic parameters of the bearings (yield strength, pre-yield stiffness, and post-yield stiffness). Considering the structural characteristics of seismic isolation continuous girder bridges, the application of PSO in parameter optimization focuses on reducing seismic impact and enhancing the adaptability of the structure, aiming to find the optimal combination of parameters that improve the performance of the bridge under seismic loading<sup>21,22</sup>.

The flowchart for solving the multi-parameter optimization problem of damping isolation bearings using the PSO algorithm is shown in Fig. 2.

While the classic PSO algorithm demonstrates considerable strength in multi-parameter bearing optimization, nonlinear and large-scale practical scenarios often require faster convergence and more adaptive search strategies. To overcome these challenges, this study proposes an improved APSO algorithm that dynamically adjusts key parameters to enhance both the optimization rate and iteration speed. These enhancements broaden the scope of swarm intelligence in seismic isolation bearing design, enabling safer and more cost-effective solutions in the complex engineering environments of earthquake-prone regions.

## Adaptive particle swarm optimization algorithm for seismic isolation bearings in bridges

Although the multi-objective PSO algorithm has gained increasing popularity in the fields of structural and seismic engineering due to its relatively simple algorithmic principles and fewer control parameters<sup>23</sup>, it still has certain limitations. Classic PSO often faces the issue of premature convergence when the search space is large and complex. The particle swarm may converge to a local optimum early in the iteration process, resulting in stagnation. If the distribution of particles in certain parameter dimensions (such as yield strength, pre-yield stiffness, or post-yield stiffness) is too narrow or uneven, the swarm may become stuck, hindering global optimization and slowing convergence.

These shortcomings highlight a core requirement in practical engineering applications: when optimizing bearing parameters, an algorithm is needed that not only converges quickly but also possesses strong global search capabilities. For bridges located in seismic zones, safety indices are crucial. Therefore, the ability to effectively avoid local optima and find better solutions within a limited computational time frame is particularly important.

To address this need, this paper proposes the Adaptive Particle Swarm Optimization (APSO) algorithm, which systematically adapts the key parameters of the particle swarm (such as inertia factor, learning factors, velocity and position update rules, and iteration termination conditions) to address these challenges. During the optimization process, APSO dynamically adjusts various parameters to provide a broader search space in the early stages (enhancing global exploration) and accelerate convergence in later stages. These improvements make APSO more suitable for practical engineering projects, allowing it to optimize faster and more robustly when dealing with multi-dimensional seismic isolation bearing parameters.

The following sections will detail the specific improvements of APSO and explain how it effectively addresses the shortcomings of classic PSO, achieving better results in multi-parameter seismic bearing optimization.

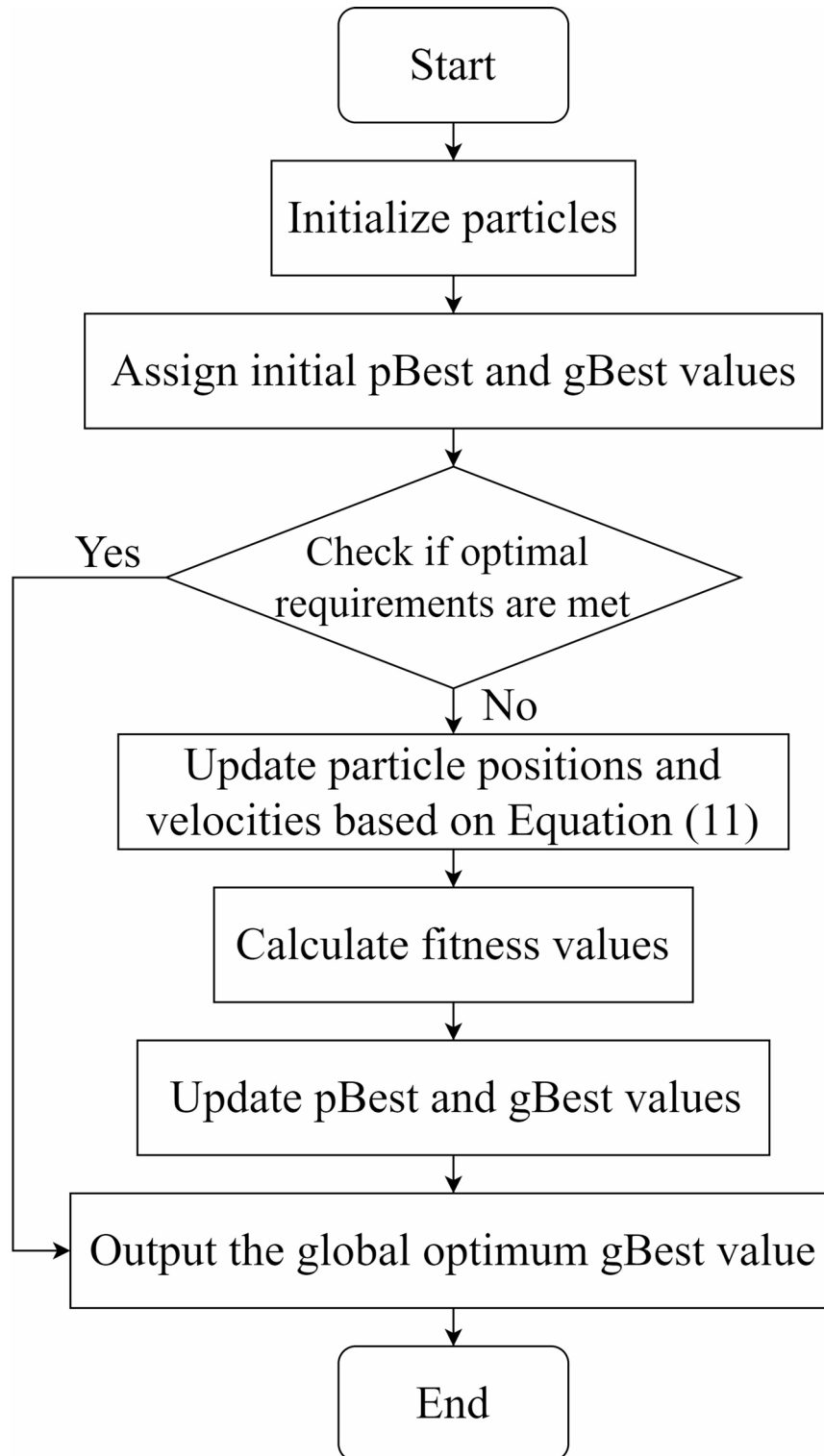


**Fig. 1.** Basic flow chart of PSO.

#### Improvement of inertia factor

It is generally believed that the inertia factor has the greatest impact on the iteration speed. The value of the inertia factor plays a crucial role in both the global search ability and the search speed of the algorithm. Since Shi introduced the linear inertia factor in 1998, many scholars have proposed different methods for assigning inertia factor values based on different problems. However, most of these methods perform well only for specific problems and lack strong general applicability<sup>24</sup>.

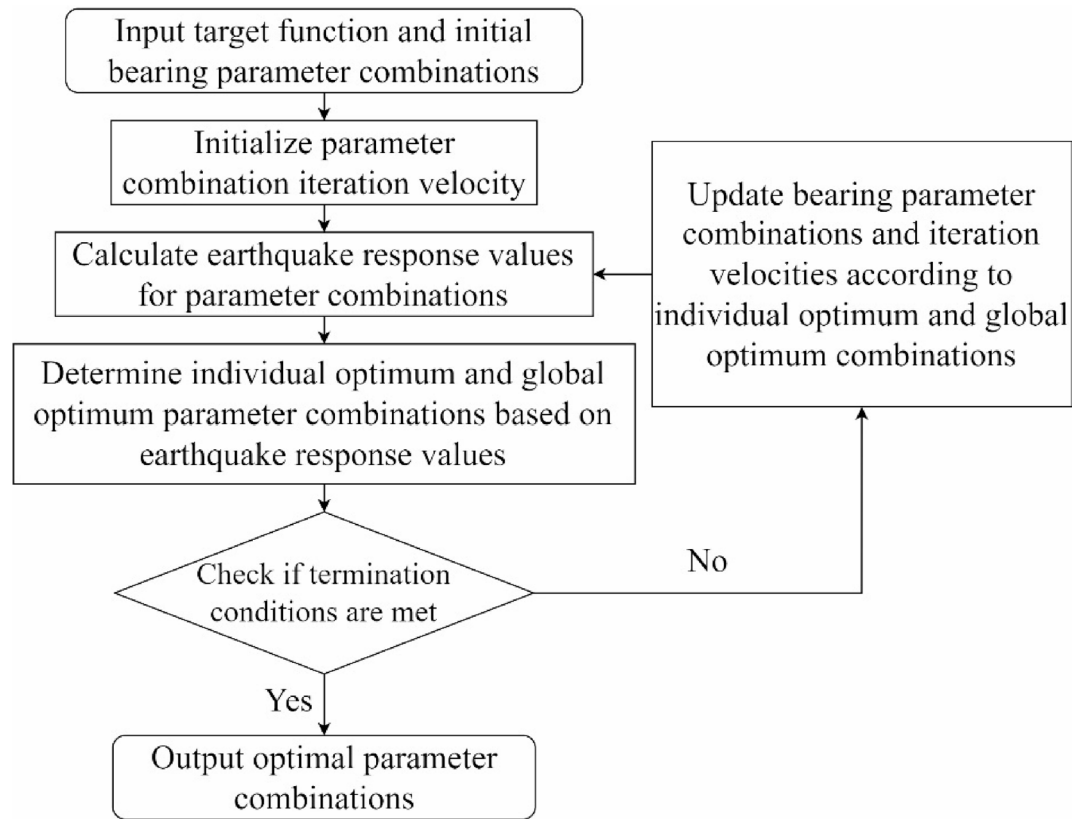


**Fig. 2.** PSO Algorithm for Solving Bearing Optimal Parameter Combinations Flowchart.

In this paper, a new adaptive inertia factor is introduced for the multi-parameter optimization of damping isolation bearings. This adaptive inertia factor allows the iteration process to decrease slowly in the early stages to expand the search range of particles, decrease more rapidly in the middle stages to improve iteration speed and efficiency, and decrease slowly in the later stages to allow particles to fine-tune their search near the optimal solution, enhancing accuracy. The use of the exponential term ensures that the adjustment of the inertia factor is smooth and continuous, facilitating better balance between exploration and exploitation throughout the optimization process. The value assignment method for this adaptive inertia factor is given by Eq. (13).

$$\omega_d = \omega_{end} + (\omega_{ini} - \omega_{end}) \times e^{[k \cdot \sigma(t)^\theta]} \quad (13)$$

where  $\sigma(t)$  is the fitness value dispersion coefficient during the iteration process;  $k$  and  $\theta$  are experimental constants determined by the initial fitness value. Typically, the optimal values are selected by conducting multiple simulations and observing the resulting search efficiency and convergence behavior of the optimization algorithm.

The fitness value dispersion coefficient is the ratio of the standard deviation to the mean value of the data set, expressed as a percentage. The common calculation formula for this is shown in Eq. (14).

$$\sigma(t) = \frac{C}{\bar{X}} \times 100\% \quad (14)$$

where  $C$  represents the data standard deviation;  $\bar{X}$  represents the data mean value.

### Improvement of learning factors

The inertia factor primarily determines the speed of the iterating particles, while the learning factor governs the learning of the individual best position and the global best position. In the standard PSO algorithm, the learning factor is usually fixed as a constant. Such a constant learning factor lacks variability and flexibility, thus having little positive impact on the algorithm. Therefore, to enhance the learning factor's positive effect, the general constant learning factor is replaced with a linear learning factor: In the early stages, to expand the search range, the emphasis should be on the influence of the individual best position; in the later stages, to more quickly and accurately find the optimal solution, the focus should shift to the influence of the global best position. Unlike the inertia factor, exponential decay usually reduces the learning factor quickly in the early stages of the optimization process, which may cause particles to be too concentrated near the global optimal solution too early, reducing the diversity of exploration. This may cause the algorithm to fall into a local optimal solution

without enough opportunities to explore the entire search space. The value assignment method for this learning factor is shown in Eq. (15).

$$\begin{cases} c_1^t = c_1^{ini} + \frac{(G_k - g)(c_1^{ini} - c_1^{end})}{G_k} \\ c_2^t = c_2^{ini} + \frac{(G_k - g)(c_2^{ini} - c_2^{end})}{G_k} \end{cases} \quad (15)$$

where  $c_1^t, c_2^t$  represent the values of the learning factors during the iteration process;  $c_1^{ini}, c_1^{end}$  are the starting and final values of the  $c_1$  learning factor;  $c_2^{ini}, c_2^{end}$  are the starting and final values of the  $c_2$  learning factor;  $G_k$  represents the maximum number of iterations;  $g$  represents the individual particles.

### Improvement of position update method

The direction and position of a particle during iteration are primarily controlled by the individual best and global best positions. This often leads to the particles becoming trapped in local optima and overlooking better positions within the particle's neighborhood. To reduce this occurrence, a certain range of neighborhood intervals,  $[pBest_i^t(1 - r(0, 1)), pBest_i^t(1 + r(0, 1))]$  and  $[gBest_i^t(1 - r(0, 1)), gBest_i^t(1 + r(0, 1))]$ , is added around the individual best and global best positions, allowing the particles to perform a neighborhood random search within these specific regions.

### Improvement of iteration termination conditions

To ensure the accuracy and feasibility of the iteration results, the condition that the difference between the maximum and minimum fitness values should not exceed 5% is combined with an additional condition: the discrete coefficient of the fitness values for all particles after each iteration must not exceed 5%. This adjustment helps optimize the final results of the iteration.

Finally, the updated particle velocity update formula is given in Eq. (16).

$$v_{id}^{t+1} = \omega_d v_{id}^t + c_1^t r_1 (pBest_{id}^t(1 \pm r(0, 1)) - x_{id}^t) + c_2^t r_2 (gBest_{id}^t(1 \pm r(0, 1)) - x_{id}^t) \quad (16)$$

The flowchart for solving the multi-parameter optimization problem of damping isolation bearings using the improved APSO algorithm is shown in Fig. 3.

## Engineering example

### Finite element model and seismic input

#### Engineering background

This study focuses on a four-span seismic isolation continuous girder bridge with a span of  $4 \times 36$  m. The superstructure of the bridge consists of a prestressed concrete box girder with a uniform cross-section, where the height of the girder is 1.8 m, and the bridge deck width is 25.7 m. The cross-section is of a single box with multiple chambers, and C50 concrete is used. The substructure consists of rectangular dual piers, each with a height of 9 m and dimensions of 1.8 m  $\times$  2 m, constructed with C40 concrete. The pile foundation uses a group of piles, with a pile diameter of 1 m and a height of 40 m, made from C30 concrete. Each pier is equipped with one bearing, except for the two end abutments, which use Y4Q520  $\times$  135G0.8 type circular lead-core rubber bearings (LRB). The abutments are equipped with LNR(H)-d445  $\times$  136 type sliding horizontal force dispersing rubber bearings (LNR). To differentiate the piers at various locations, the bridge is numbered sequentially along the bridge direction as Pier 1#, Pier 2#, and Pier 3#. The longitudinal profile and plan layout of the bridge are shown in Figs. 4 and 5.

#### Support bilinear model

In the Midas software, the simulation of LRB bearings can directly use the linear characteristics of lead-core rubber bearings from the general connection characteristic values provided by the software. The simulation of the LNR bearings can be directly modeled using elastic connections. The equivalent linearization model represents the lead core rubber bearing as an approximate linear model, consisting of two linear mechanical parameters: equivalent stiffness and equivalent damping ratio. Such models are typically used for response spectrum analysis within the elastic range of structures<sup>25</sup>. When subjected to external cyclic loading, the deformation of the lead core rubber bearing remains within the elastic-plastic range, and thus, the restoring force of the bearing is often modeled as bilinear<sup>26</sup>. A common bilinear model for lead core rubber bearings is shown in Fig. 6. The calculation formulas for the equivalent stiffness and equivalent damping ratio are given in Eqs. (17) and (18), respectively.

$$K_{eff} = \frac{F_d}{D_d} = \frac{Q_d}{D_d} + K_2 \quad (17)$$

$$\xi_{eff} = \frac{2Q_d(D_d - \Delta_y)}{\pi D_d^2 K_{eff}} \quad (18)$$

where  $D_d$  represents the horizontal displacement of the seismic isolation bearing. According to the provisions of "Lead Core Seismic Isolation Rubber Bearings for Highway Bridges", the  $D_d$  value is taken as 50 mm;  $\Delta_y$  is the yield displacement of the seismic isolation bearing;  $Q_d$  is the characteristic strength of the seismic isolation bearing, defined as the value where the hysteresis curve intersects the shear force axis in the forward direction;  $K_{eff}$  denotes the equivalent stiffness of the seismic isolation bearing;  $K_1$  is the pre-yield stiffness of the seismic

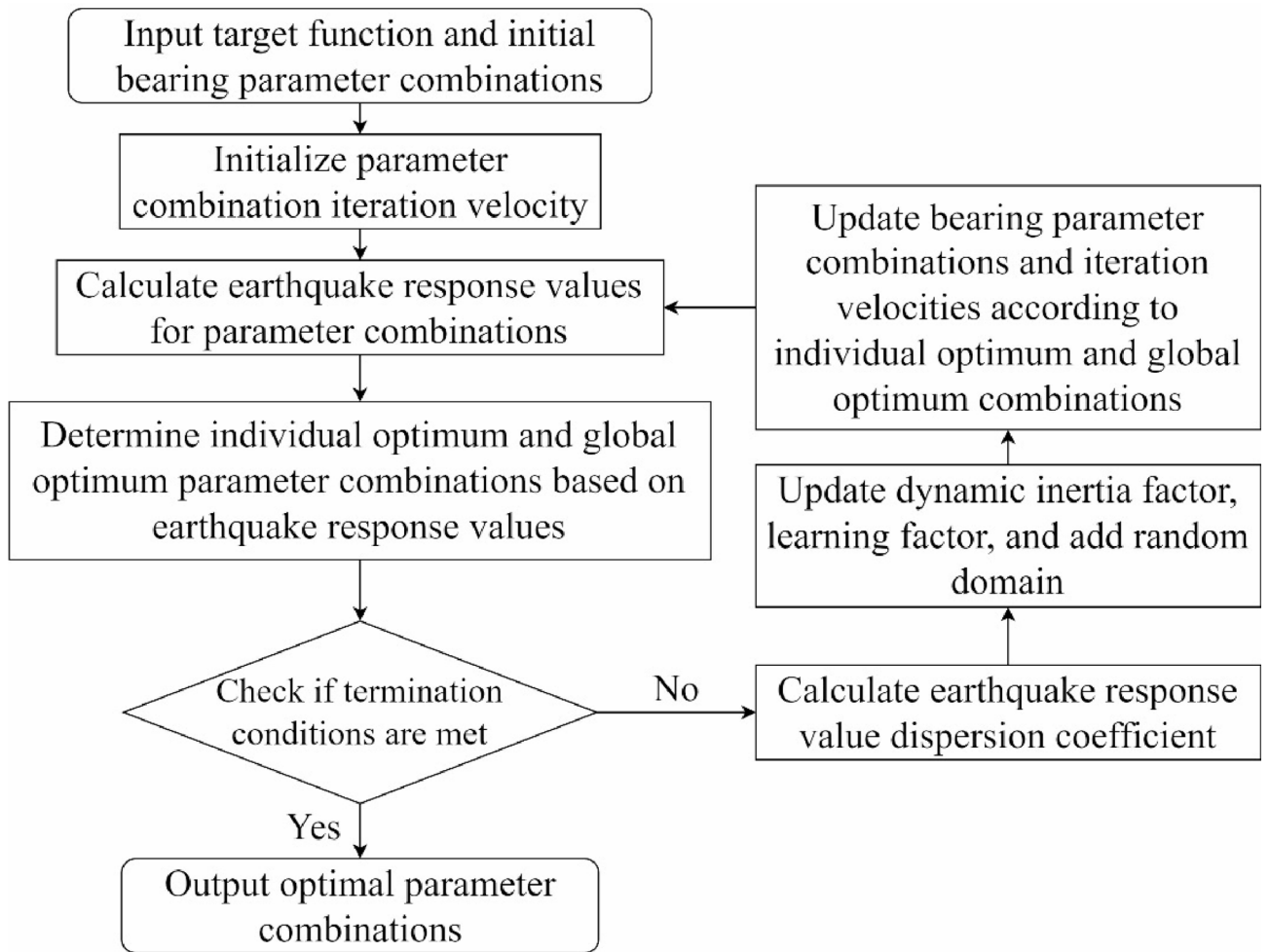


Fig. 3. APSO algorithm for solving bearing optimal parameter combinations flowchart.

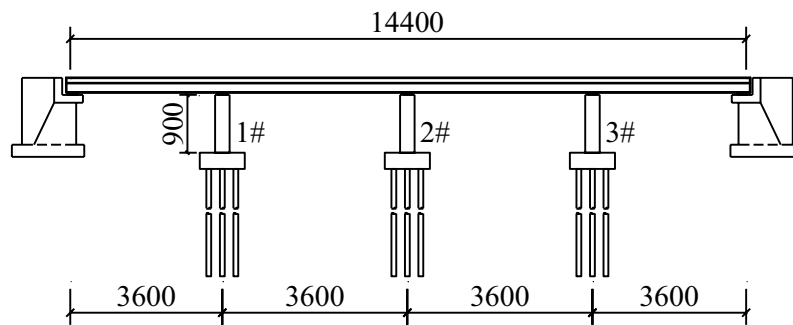


Fig. 4. Bridge longitudinal section layout (unit: cm).

isolation bearing;  $K_2$  is the post-yield stiffness of the seismic isolation bearing;  $\xi_{eff}$  represents the equivalent damping ratio of the seismic isolation bearing.

As shown in Fig. 6, the behavior of the lead core rubber bearing can be characterized by four parameters in the restoring force model: yield strength, equivalent stiffness, elastic stiffness, and yield stiffness.

The restoring force in the bilinear model is calculated in two stages, with the formulas given in Eqs. (19) and (20).

Pre-yield stage:

$$F_b = (K_1 - K_2)(D_d - \Delta_y) + K_2 D_d \tag{19}$$

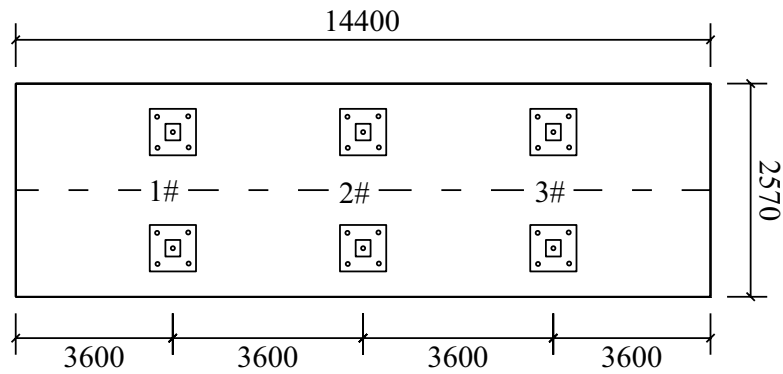


Fig. 5. Bridge plan layout (unit: cm).

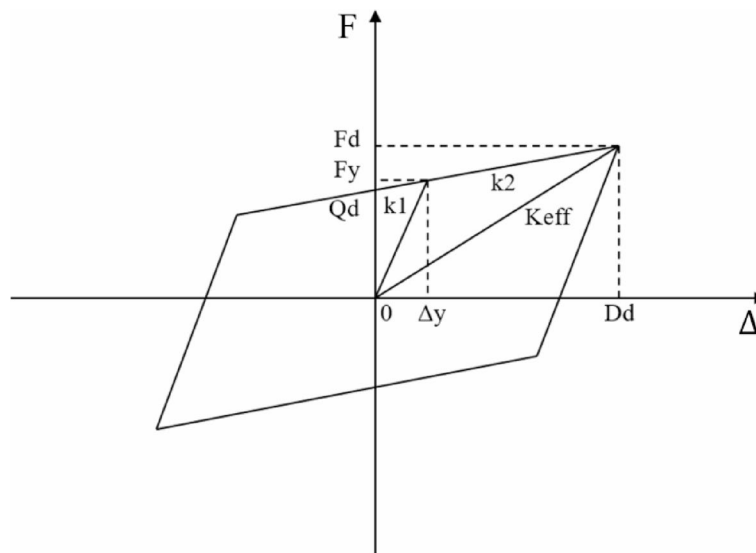


Fig. 6. Finite element analysis model.

Post-yield stage:

$$F_b = (K_1 - K_2)(D_d - \Delta_y) + K_2 D_d \tag{20}$$

where  $F_b$  represents the bearing’s restoring force.

In the Midas simulation, when using the response spectrum method for bearing simulation analysis, the software calls its linear characteristic values, including equivalent stiffness ( $K_{eff}$ ) and vertical stiffness ( $K_v$ ). Detailed parameter inputs for the bearing’s linear characteristics can be referenced from the Midas Civil help file. The implementation of the bearing bilinear model and the finite element analysis model schematic in Midas are shown in Fig. 7.

In addition, it is important to acknowledge that the simulation accuracy of seismic isolation bearings significantly influences the reliability and precision of the structural analysis results. Figure 7 presents the finite element model of bearings, adopting a bilinear constitutive model in the Midas software. However, the simplifications inherent in these simulations—particularly the potential neglect of certain complex behaviors such as the “jumping-off” effect in friction pendulum bearings—could impact the predicted performance and optimization outcomes. Recent research has highlighted that neglecting this phenomenon may lead to deviations in evaluating bearing responses under seismic excitation. For instance, the study by Wei et al.<sup>27</sup>, emphasizes that accurate modeling of the jumping-off effect significantly improves the precision of response predictions and contributes to more robust parameter optimization. Although the current approach provides acceptable accuracy within the linear and bilinear modeling assumptions, incorporating refined nonlinear behaviors could further validate the optimization results and extend the applicability of findings to practical engineering scenarios. Thus, while the current simulations in Fig. 7 meet the immediate objectives, recognizing and addressing these complex bearing behaviors could substantially enhance the comprehensiveness and reliability of seismic isolation performance analyses.

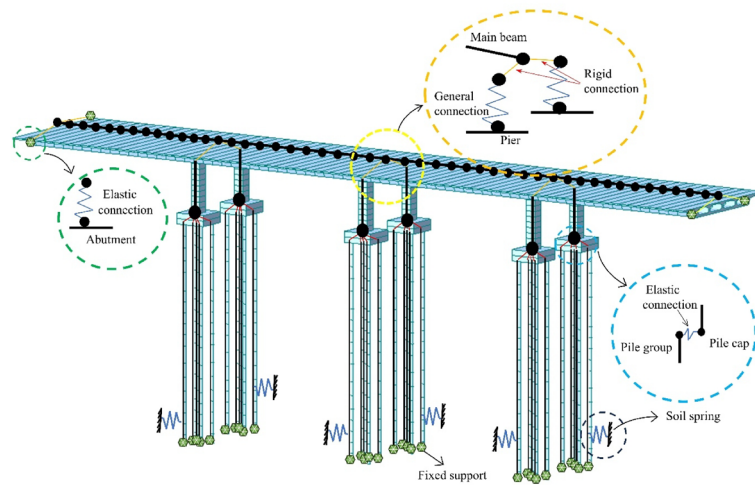


**Fig. 7.** Finite element analysis model.

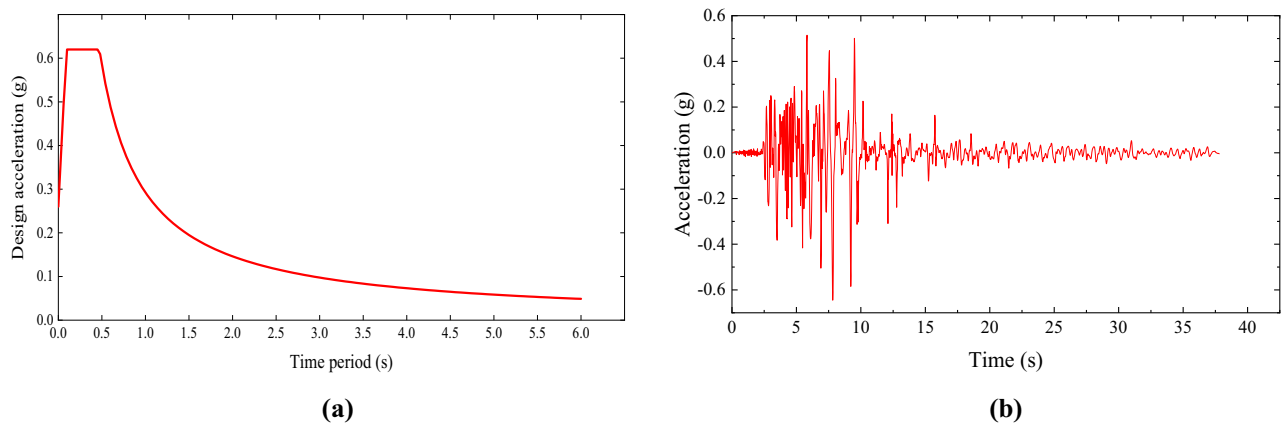


**Fig. 8.** James's earthquake wave. (a) target response spectrum. (b) earthquake time history excitation.

#### Earthquake input

This study uses the “Seismic Design Code for Highway Bridges” (JTJ/T2231-01-2020) to plot the design response spectrum, which serves as the target spectrum, as shown in Fig. 8. The seismic isolation continuous beam bridge selected in this paper is located at a site with a basic earthquake intensity of 8 degrees and a site category of Class III. According to the regulations, the vertical earthquake effect is not considered. According to the code, the acceleration time history should consist of no fewer than three sets. Therefore, three earthquake waves—James, Imperial Valley-01, and Parkfield—were selected from the PEER strong-motion database. Among the earthquake responses caused by these three waves, the James earthquake wave induces the maximum seismic response in the bridge. Consequently, this study analyzes the parameter optimization of the pre-yield stiffness of the bearings under the effect of this seismic wave. The evaluation criteria for the optimization include the pier top displacement, pier bottom shear force, and their weighted sum. The time history of the acceleration at the pier top is shown in Fig. 8.

#### Single-parameter sensitivity-based optimization of seismic isolation bearing parameters

To investigate the impact of various bearing parameters on the seismic performance of continuous girder bridges, this section uses a single-parameter sensitivity analysis under the James earthquake excitation. Specifically, one parameter (yield strength, pre-yield stiffness, or post-yield stiffness) is adjusted at a time while keeping the other parameters constant. The impact of these changes on the bridge's seismic performance is then evaluated. Although practical bridge design requires the evaluation of multiple earthquake waves, to visually demonstrate the impact of a single parameter on isolation effectiveness, this study selects the James earthquake wave as the focus of the analysis and optimizes each parameter individually.

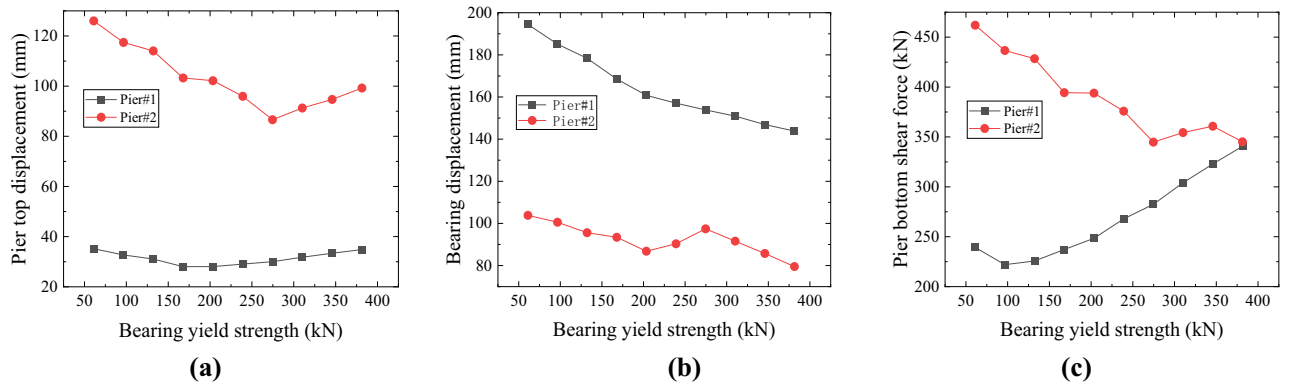


**Fig. 9.** Bridge seismic response under different bearing yield strengths. (a) pier top displacement. (b) bearing displacement. (c) pier bottom shear force.

Optimization objective	Optimal yield strength (kN)	Resulting displacement (mm)	Resulting shear force (kN)	Displacement reduction (%)	Shear force reduction (%)
Minimize pier top displacement	274.6	293.26	-	21.17%	-
Minimize bearing displacement	167.8	-	1450.4	-	18.27%
Balanced shear-displacement	167.8	318.58	1450.4	14.36%	18.27%

**Table 1.** Optimization effects on seismic response at optimal yield strengths. At this point, the bearing’s pre-yield stiffness is 9.3 kN/mm, and post-yield stiffness is 1.4 kN/mm.

*Design principles and parameter settings*

Before analyzing the impact of individual parameters, some design principles and parameter ranges need to be established. The finite element model used in this section is the same as the one in Sect. 4.1, which includes the bridge’s geometric dimensions, material properties, and boundary conditions. The seismic input is based on the James earthquake record, adjusted according to relevant seismic design standards to represent a high-intensity seismic scenario<sup>28</sup>.

In the nonlinear behavior of lead-core rubber bearings (LRB), three key parameters are crucial:

- (1) Yield Strength ( $Q_y$ ): This determines the energy dissipation capacity of the bearing, with a value range of 61 kN to 381.4 kN, with a step size of 35.6 kN.
- (2) Pre-Yield Stiffness ( $K_1$ ): This affects the elastic response of the bearing and the structural natural frequency, with a range of 4.5 kN/mm to 18.5 kN/mm, with a step size of 1.4 kN/mm.
- (3) Post-Yield Stiffness ( $K_2$ ): This reflects the bearing’s mechanical performance in the post-yield stage, with a value range of 0.7 kN/mm to 2.95 kN/mm, with a step size of 0.25 kN/mm.

For ease of comparison, this section extracts absolute values closely related to seismic performance (such as pier top displacement, bearing displacement, and pier bottom shear force) from the time history analysis results. These values are normalized when necessary to highlight the relative impact of parameter changes.

*Bridge seismic response and bearing parameter optimization under different yield strengths*

In this section’s single-parameter sensitivity analysis, the yield strength  $Q_y$  is varied over ten different values while holding other bearing parameters constant. Time history analysis is performed using the James earthquake record. As shown in Fig. 9, as  $Q_y$  increases, the pier top displacement decreases within a certain range. However, once the yield strength exceeds a certain threshold, it starts to increase again, indicating that moderate yield strength is beneficial for energy dissipation, while excessively high stiffness redirects more seismic force to the superstructure. Meanwhile, bearing displacement generally decreases as  $Q_y$  increases and remains within the allowable shear deformation range. This trend is also reflected in the distribution of pier bottom shear forces, where larger  $Q_y$  values reduce the force difference between the high pier (Pier #2) and the low pier (Pier #1), leading to a more balanced seismic force distribution across the bridge piers.

Based on these results, this study minimizes the pier top displacement, minimizes the pier bottom shear force, and uses a weighted combination of both as objectives for the single-parameter optimization under the James earthquake. Table 1 lists the optimal values for each objective and the corresponding improvements relative to the original design of Y4Q520 × 135G0.8. When  $Q_y \approx 274.6\text{ kN}$ , the pier top displacement decreases by approximately 21.17%, while  $Q_y \approx 167.8\text{ kN}$  results in an 18.27% reduction in pier bottom shear force. The weighted combination of displacement and shear force results in reductions of 14.36% and 18.27%, respectively.

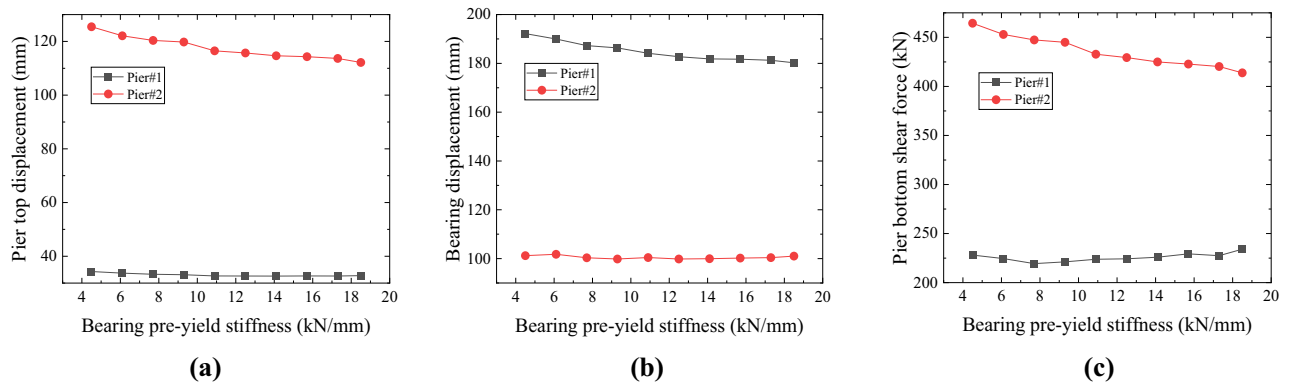


**Fig. 10.** Bridge seismic response under different pre-yield stiffness of bearings. (a) pier top displacement. (b) bearing displacement. (c) pier bottom shear force.

Optimization objective	Optimal yield strength (kN)	Resulting displacement (mm)	Resulting shear force (kN)	Displacement reduction (%)	Shear force reduction (%)
Minimize pier top displacement	18.5	355.4	-	4.46%	-
Minimize bearing displacement	17.3	-	1750.6	-	1.36%
Balanced shear-displacement	17.3	357.88	1750.6	3.8%	1.36%

**Table 2.** Optimization effects on seismic response at pre-yield stiffness. At this point, the bearing yield strengths is 96 kN/mm, and post-yield stiffness is 1.4 kN/mm.

These results demonstrate that moderate yield strength achieves a balance between energy dissipation and pier bottom force, providing a more uniform force distribution and improved seismic performance for the continuous girder bridge under strong seismic excitation.

*Bridge seismic response and bearing parameter optimization under pre-yield stiffness*

When analyzing the pre-yield stiffness ( $K_1$ ), ten different values for  $K_1$  were set while holding other bearing parameters constant, and time history analysis was conducted using the James earthquake record. As shown in Fig. 10, with increasing  $K_1$ , the pier top displacement shows a linear decreasing trend, and bearing displacement slightly decreases, remaining within the allowable deformation range. This indicates that larger  $K_1$  effectively enhances the initial stiffness of the bearing while avoiding excessive deformation. Regarding pier bottom shear force, Pier #1 is less affected by  $K_1$ , while Pier #2 shows a significant reduction in shear force as  $K_1$  increases. This suggests that for relatively taller piers, greater initial stiffness better resists lateral seismic forces.

Since the James earthquake induces the strongest excitation among the selected waveforms, the single-parameter optimization aimed to minimize pier top displacement, minimize pier bottom shear force, and minimize the weighted combination of both. The final results are shown in Table 2. When  $K_1 \approx 18.5\text{ kN/mm}$ , the pier top displacement decreases by about 4.46% compared to the original design of Y4Q520×135G0.8.  $K_1 \approx 17.3\text{ kN/mm}$  is more favorable for reducing pier bottom shear force (1.36%) and provides a balanced control over both displacement and force in the weighted objective. Although the improvements are not significant, they highlight the fine-tuning effect of pre-yield stiffness on the bridge’s initial seismic response and suggest that even small adjustments to  $K_1$  may lead to a more reasonable seismic force distribution between tall and short piers.

*Bridge seismic response and bearing parameter optimization under pre-yield stiffness*

In this section, the impact of post-yield stiffness  $K_2$  on the seismic performance of the continuous girder bridge under the James earthquake is examined. As shown in Fig. 11, the pier top displacement increases almost linearly with  $K_2$ , while bearing displacement initially decreases with increasing  $K_2$ , reaching a turning point near  $K_2 \approx 2.2\text{ kN/mm}$ , and then increases again. At the same time, pier bottom shear force continues to increase with  $K_2$ . Although these response curves do not show clear minima or maxima within the test range, bearing displacement remains below its ultimate shear capacity, indicating that stiffness variations within this range will not cause the bearings to exceed the safe deformation limits.

Table 3 shows that when  $K_2 \approx 0.7\text{ kN/mm}$ , the displacement and shear force improve by approximately 9.96% and 13.68%, respectively, compared to the original design of Y4Q520×135G0.8. Although these improvements are not substantial, they emphasize the critical role of post-yield stiffness in seismic force

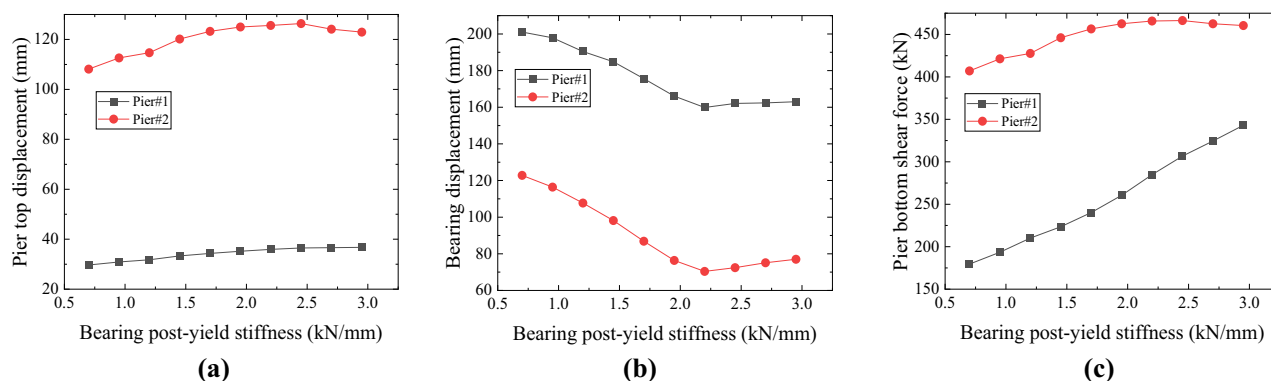


**Fig. 11.** Bridge seismic response under different post-yield strengths of bearings. (a) pier top displacement. (b) bearing displacement. (c) pier bottom shear force.

Optimization objective	Optimal yield strength (kN)	Resulting displacement (mm)	Resulting shear force (kN)	Displacement reduction (%)	Shear force reduction (%)
Minimize pier top displacement	0.7	334.96	-	9.96%	-
Minimize bearing displacement	0.7	-	1532	-	13.68%
Balanced shear-displacement	0.7	334.96	1532	9.96%	13.68%

**Table 3.** Optimization effects on seismic response at post-yield stiffness. At this point, the bearing yield strengths is 96 kN/mm, and pre-yield stiffness is 9.3 kN/mm.

Factors	Values at different levels		
	Level 1	Level 2	Level 3
Yield strength (kN)	140	220	300
Pre-yield stiffness (kN/mm)	8	11.5	15
Post-yield stiffness (kN/mm)	1.26	1.83	2.4

**Table 4.** Orthogonal test factor levels.

distribution. If  $K_2$  is too high, it increases the displacement demand on the bridge piers, while moderately lower  $K_2$  is more advantageous in achieving a balanced control between deformation and reduced force.

### Multi-parameter optimization of seismic isolation bearings based on orthogonal experiment

#### Principles of orthogonal experiment

The orthogonal experimental method provides a systematic framework for exploring the optimal combination of multiple parameters. In seismic isolation bearing design, three critical parameters—yield strength, pre-yield stiffness, and post-yield stiffness—often interact with one another. By selecting representative levels for the parameters and arranging them in an orthogonal table, it is possible to significantly reduce the number of simulations required while maintaining the robustness of the optimization results. The orthogonal experiment primarily revolves around the use of orthogonal tables, which combine different values of bearing parameters through orthogonal combinations. This ensures that each non-linear characteristic parameter appears evenly across all possible combinations, allowing each parameter to independently influence the optimization results and enabling the identification of the optimal parameter combination. Orthogonal tables are typically denoted as  $L_n(b^c)$ , where  $L$  represents the orthogonal table,  $n$  represents the total number of experiments,  $c$  represents the number of factors under consideration, and  $b$  represents the number of levels of each factor. Factors refer to the specific parameters that influence the experimental results—in this case, the non-linear characteristic parameters of the bearings; levels refer to the specific values of these factors—here, the specific values of the bearing’s non-linear characteristics. In this study, range analysis is primarily used to evaluate the impact of each factor on the experimental results.

#### Parameter settings

The numerical model and the range of values for the bearing’s non-linear characteristic parameters are the same as those in Sect. 4.2. The factors and their levels used in this orthogonal experiment are shown in Table 4.

Test number	Factors		
	Yield strength (kN)	Pre-yield stiffness (kN/mm)	Post-yield stiffness (kN/mm)
1	140	8	1.26
2	140	11.5	2.4
3	140	15	1.83
4	220	8	2.4
5	220	11.5	1.83
6	220	15	1.26
7	300	8	1.83
8	300	11.5	1.26
9	300	15	2.4

**Table 5.** Orthogonal table for bearing nonlinear characteristic parameters.

Test number	Evaluation indicators		
	Pier top displacement (mm)	Pier bottom shear force (kN)	Weighted sum of both
1	332.29	1699.3	0.73
2	364.81	2061.28	1.81
3	341.3	1814.1	1.06
4	356.74	2155.6	1.91
5	321.86	1934.58	1.09
6	272.7	1659.1	0
7	330.62	2075.72	1.47
8	298.16	1775.24	0.51
9	350.17	2128.74	1.79

**Table 6.** The evaluation index and calculation result are analyzed by orthogonal experiment.

	Level	Factor 1(yield strength)	Factor 2(pre-yield stiffness)	Factor 3(post-yield stiffness)
$K_i$ value	1	1038.39	1019.65	903.15
	2	951.3	984.82	993.77
	3	978.94	964.16	1071.72
$\bar{K}_i$ value	1	346.13	339.88	301.05
	2	317.1	328.27	331.26
	3	326.31	321.39	357.24
Optimal level	1	2	3	
R value	135.01	29.03	18.5	

**Table 7.** The results of range analysis with pier top displacement as the evaluation index.

Based on these values, a 3-factor, 3-level orthogonal table.  $L_9(3^3)$  is employed for the experiment, with the specific orthogonal design shown in Table 5. According to the orthogonal table, only 9 simulations are required for the three-factor, three-level simulation experiments, significantly reducing the workload.

#### *Multi-parameter optimization of seismic isolation bearings for continuous girder bridges*

For the seismic design optimization based on the seismic responses induced by three earthquake waves, the James earthquake wave, which induces the largest seismic response among the three, is selected for this section. The time history analysis method is used to optimize the bearing parameters, with the evaluation criteria being the pier top displacement, pier bottom shear force, and the weighted sum of both. The results of the orthogonal experiment analysis and calculations for the seismic isolation linear continuous girder bridge are shown in Table 6.

Range analysis is performed for different evaluation criteria and calculation results. The analysis results are as follows:

- (1) The range calculation results for the pier top displacement as the evaluation criterion are shown in Table 7.

Yield strength (kN)	Pre-yield stiffness (kN/mm)	Post-yield stiffness (kN/mm)	Resulting displacement (mm)	Optimization rate
220	15	1.26	272.7	26.69%

**Table 8.** Optimal parameter combinations and optimization rates for bearings.

	Level	Factor 1(yield strength)	Factor 2(pre-yield stiffness)	Factor 3(post-yield stiffness)
$K_i$ value	1	5574.68	5930.62	5133.64
	2	5749.28	5771.1	5824.4
	3	5979.7	5601.94	6345.62
$\bar{K}_i$ value	1	1858.23	1976.87	1711.21
	2	1916.43	1923.7	1941.47
	3	1993.23	1867.31	2115.21
Optimal level	1		3	1
R value		135.01	109.56	403.99

**Table 9.** Range analysis results for pier bottom shear force as the evaluation indicator.

Yield strength (kN)	Pre-yield stiffness (kN/mm)	Post-yield stiffness (kN/mm)	Resulting displacement (mm)	Optimization rate
140	15	1.26	1594.64	10.15%

**Table 10.** The combination of the optimal parameters of the support and the optimization rate.

	Level	Factor 1(yield strength)	Factor 2(pre-yield stiffness)	Factor 3(post-yield stiffness)
$K_i$ value	1	3.6	4.11	1.24
	2	3	3.41	3.61
	3	3.77	2.84	5.51
$\bar{K}_i$ value	1	1.2	1.37	0.41
	2	1	1.14	1.2
	3	1.26	0.95	1.84
Optimal level	2		3	1
R value		0.25	0.42	1.42

**Table 11.** Results of parameter optimization with shear force-displacement weighted sum as the target function.

The optimal parameter combinations for the bearings under the orthogonal experiment, based on the pier top displacement, and the optimization rate relative to the original engineering bearing Y4Q520×135G0.8 are shown in Table 8.

(2) The range calculation results for the pier bottom shear force as the evaluation criterion are shown in Table 9.

The optimal parameter combinations for the bearings under the orthogonal experiment, based on pier bottom shear force, and the optimization rate relative to the original engineering bearing Y4Q520×135G0.8 are shown in Table 10.

(3) The range calculation results for the weighted sum of shear force and displacement as the evaluation criterion are shown in Table 11.

The optimal parameter combinations for the bearings under the orthogonal experiment, based on the weighted sum of shear force and displacement, and the optimization rate relative to the original engineering bearing Y4Q520×135G0.8 are shown in Table 12.

In summary, the seismic response of the seismic isolation linear girder bridge with the optimal parameter combinations obtained through the orthogonal experiment shows a significant reduction. Compared to the original engineering bearing Y4Q520×135G0.8, the pier top displacement decreases by 26.69% when using displacement as the evaluation criterion; the shear force decreases by 10.15% when using pier bottom shear force as the evaluation criterion; and the weighted sum of displacement and shear force shows a reduction of 10.15% in displacement and 6.52% in shear force. The optimization effect is clear. Compared to parameter

Yield strength (kN)	Pre-yield stiffness (kN/mm)	Post-yield stiffness (kN/mm)	Resulting displacement (mm)	Resulting shear force (kN)	Displacement reduction (%)	Shear force reduction (%)
220	15	1.26	272.7	1659.1	10.15%	6.52%

**Table 12.** Optimal parameter combinations and optimization rates for bearings.

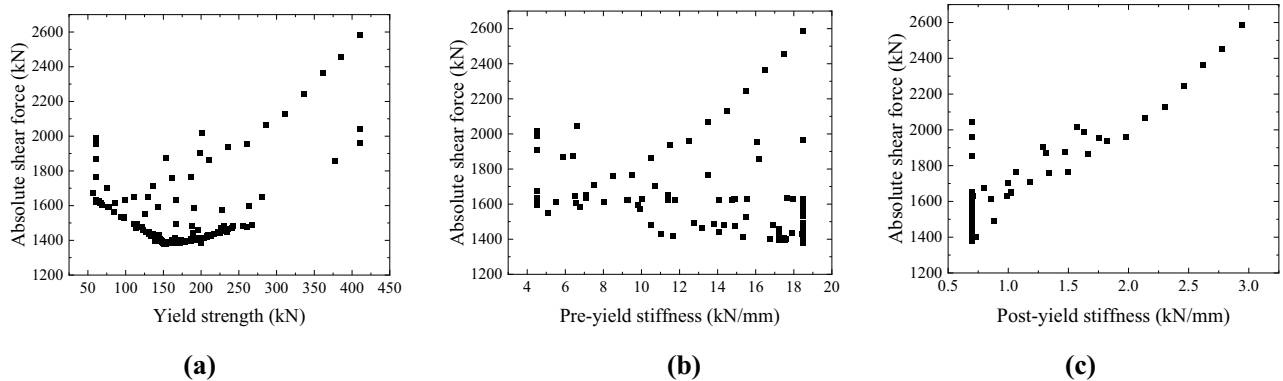


**Fig. 12.** The distribution of iterative particles projected in different directions in shear optimization space. (a) yield strength direction. (b) pre-yield stiffness direction. (c) post-yield stiffness direction.

optimization using single-parameter sensitivity analysis, the multi-parameter optimization of the bearing using the orthogonal experiment yields better results and significantly reduces the workload.

### Multi-parameter optimization of seismic isolation bearings based on the APSO algorithm

#### *Bearing multi-parameter optimization with pier bottom shear force as the objective function*

To verify the effectiveness and applicability of the APSO algorithm for multi-parameter optimization of seismic isolation bearings, this section employs time-history analysis under the James earthquake excitation. The APSO algorithm is used to iteratively optimize 15 initial bearing parameter combinations for a linear seismic isolation continuous girder bridge, with the objective function defined as the pier bottom shear force. This iterative process creates an optimization space within which the optimal parameter combination is identified to refine the bearing parameters further. To visually represent the distribution of particles in the optimization space, the projections of particles along different parameter directions are illustrated as scatter plots (see Fig. 12).

It is observed that the projection in the yield strength direction forms a V-shape, with particles gradually concentrating around  $150\text{ kN}$ ; the projection in the pre-yield stiffness direction converges toward the maximum value of  $18.5\text{ kN/mm}$ ; and the projection in the post-yield stiffness direction converges toward the minimum value of  $0.7\text{ kN/mm}$ . This uniform distribution indicates that the particle swarm covers nearly the entire parameter range during optimization. To further demonstrate the iterative paths and results, the trajectories of selected particles (8 randomly chosen for clarity) are plotted as line graphs in Fig. 13.

Based on the APSO algorithm, Table 13 presents the optimal bearing parameter combinations—using pier bottom shear force as the objective function—and their corresponding optimization rates relative to the original engineering bearing Y4Q520 × 135G0.8.

From Fig. 13; Table 13, it is evident that:

- (1) Except for the yield strength direction, where convergence is relatively slow (particles begin converging around the 20th iteration and essentially converge by the 25th), the pre-yield and post-yield stiffness directions achieve convergence more rapidly (approximately by the 15th and 4th iterations, respectively). This difference indicates that convergence in the yield strength direction is the slowest and plays a decisive role in the final optimization outcome.
- (2) The objective function stabilizes after roughly 20 iterations. Compared to the initial parameter combinations, the optimized parameters reduce the absolute value of the pier bottom shear force by 15% at minimum and up to 43% at maximum; relative to the original bearing Y4Q520 × 135G0.8, the reduction is about 22.2%, demonstrating a significant improvement.

#### *Bearing multi-parameter optimization with pier top displacement as the objective function*

Under the same James earthquake excitation and using time-history analysis, this section applies the APSO algorithm to iteratively optimize 15 initial bearing parameter combinations for the linear seismic isolation continuous girder bridge, with the objective function defined as the pier top displacement. An optimization space is thereby established for identifying the optimal parameter combination. To intuitively display the

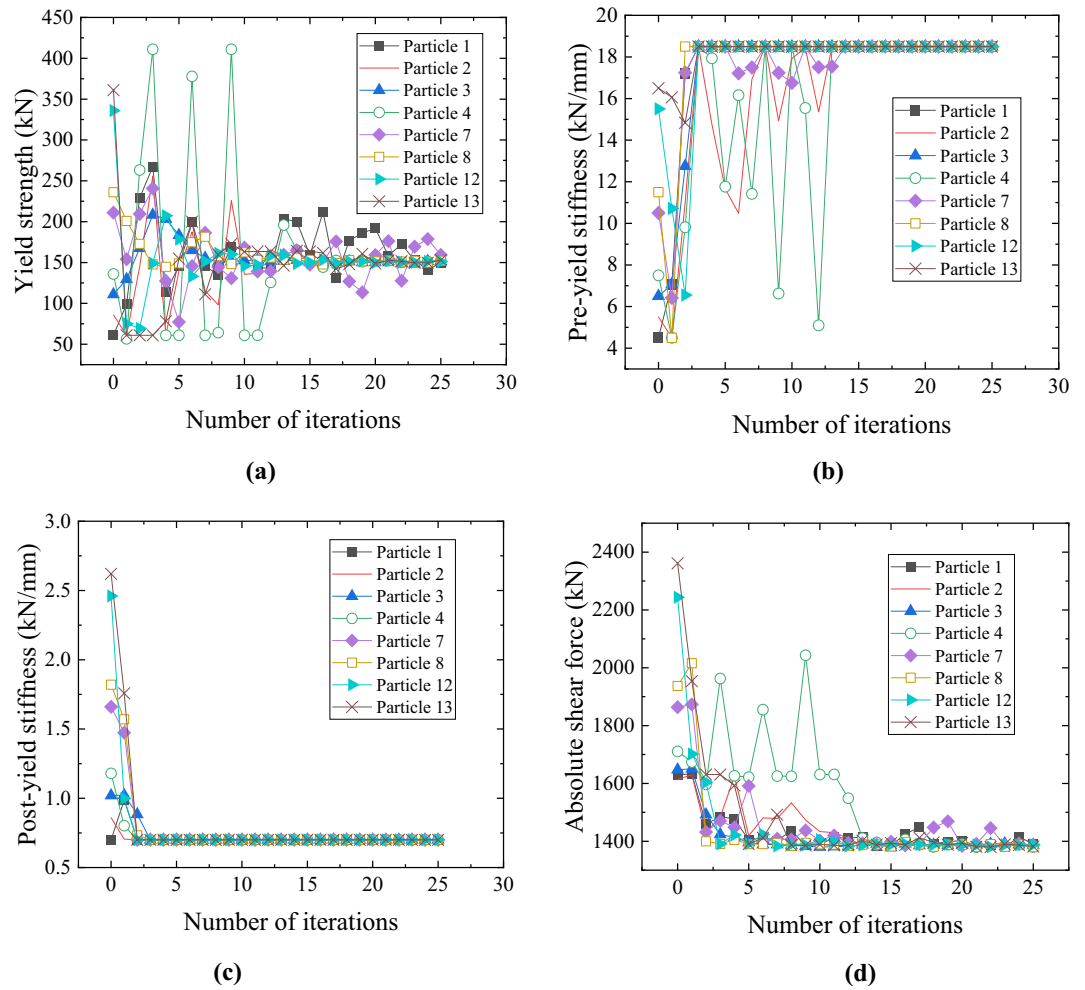


**Fig. 13.** Iteration particle projections along parameter directions in the optimization space. (a) yield strength direction. (b) pre-yield stiffness direction. (c) post-yield stiffness direction. (d) objective function value direction.

Yield strength (kN)	Pre-yield stiffness (kN/mm)	Post-yield stiffness (kN/mm)	Resulting displacement (mm)	Optimization rate
150	18.5	0.7	1378.4	22.2%

**Table 13.** The optimal parameter combination and optimization rate of the support.

distribution of particles in the optimization space, scatter plots of particle projections along different parameter directions are provided (see Fig. 14).

The results show that:

- (1) The improved APSO algorithm enables particles to search a broader parameter space with a more uniform distribution, effectively avoiding local optima and accelerating the discovery of the global optimum.
- (2) In the yield strength direction, the particle distribution exhibits a V-shape with convergence around  $210kN$ ; in the pre-yield stiffness direction, particles concentrate at the maximum value of  $18.5kN/mm$ ; and in the post-yield stiffness direction, they converge toward the minimum value of  $0.7kN/mm$ .

For clarity, the iterative trajectories of 8 randomly selected particles are depicted in Fig. 15.

Table 14 presents the optimal parameter combinations obtained with pier top displacement as the objective function, along with the corresponding optimization rates relative to the original bearing Y4Q520 × 135G0.8.

Analysis of Fig. 15; Table 14 reveals that:

- (1) Although convergence in the yield strength direction remains slower, starting around the 10th iteration and essentially converging by the 15th iteration, the pre-yield stiffness and post-yield stiffness directions

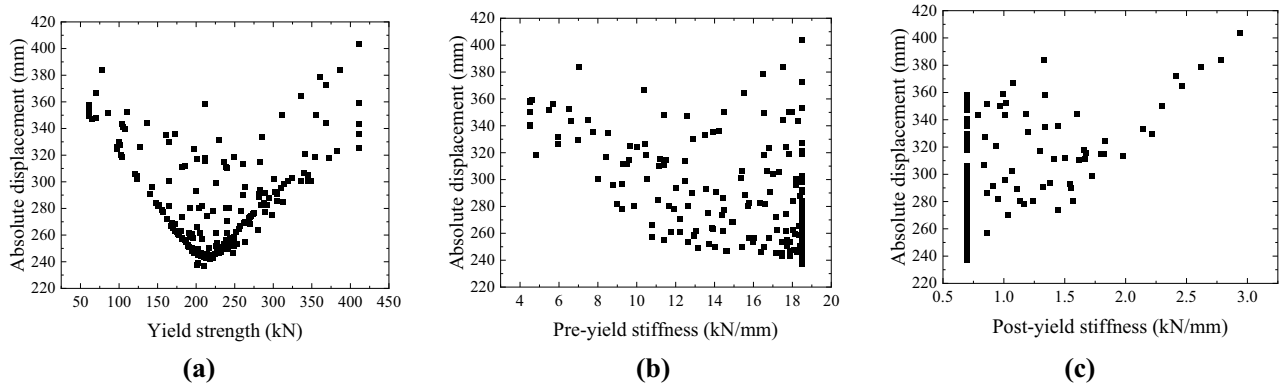


**Fig. 14.** The distribution of iterative particles projected in different directions in displacement optimization space. (a) yield strength direction. (b) pre-yield stiffness direction. (c) post-yield stiffness direction.

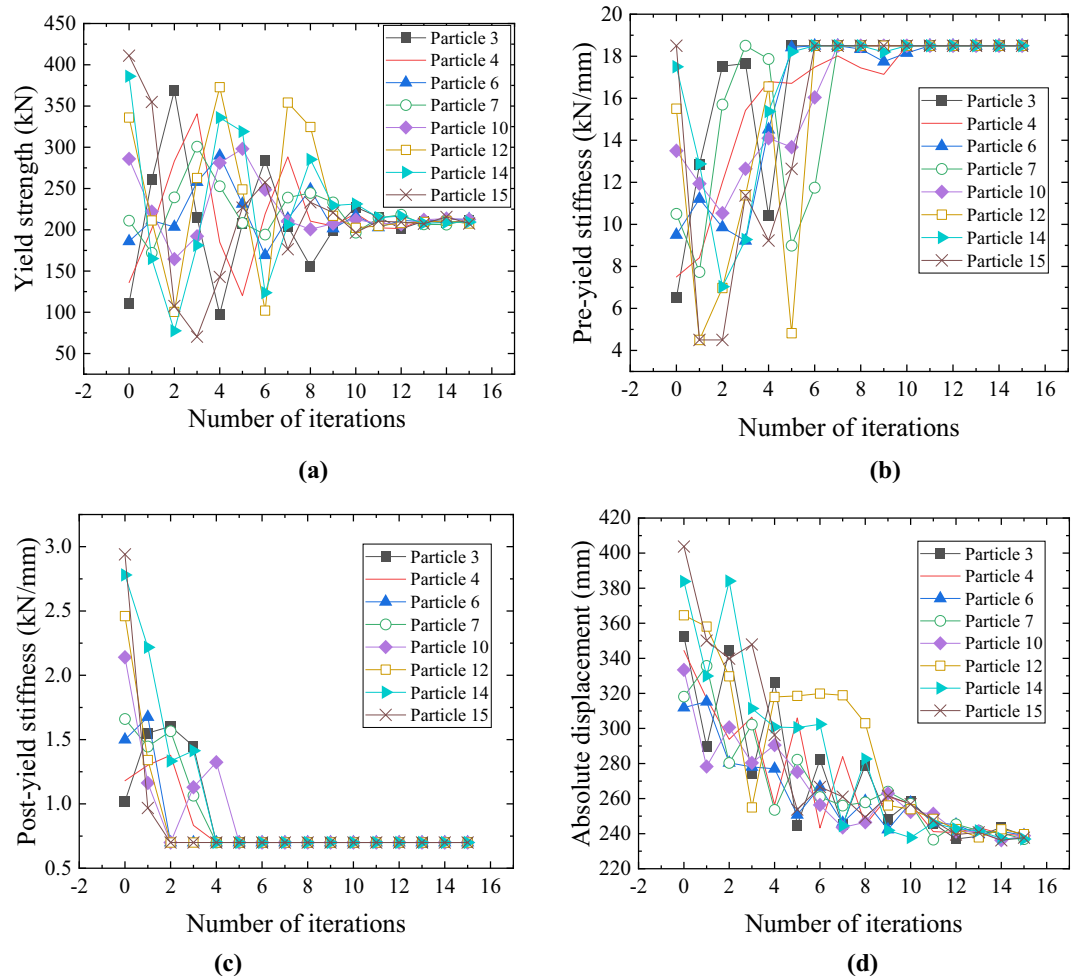


**Fig. 15.** Iteration particle projections along parameter directions in the optimization space. (a) yield strength direction. (b) pre-yield stiffness direction. (c) post-yield stiffness direction. (d) objective function value direction.

converge by approximately the 10th and 5th iterations, respectively. Overall, the total number of iterations is greatly reduced, resulting in an approximate 40% increase in convergence speed.

- (2) The objective function stabilizes after about 11 iterations, with an overall convergence speed improvement of approximately 45%. Compared to the initial parameter combinations, the optimized parameters reduce the absolute pier top displacement by 23.8% at minimum and 41.2% at maximum; relative to the original

Yield strength (kN)	Pre-yield stiffness (kN/mm)	Post-yield stiffness (kN/mm)	Resulting displacement (mm)	Optimization rate
210	18.5	0.7	236.96	36.6%

**Table 14.** The optimal parameter combination and optimization rate of the support.

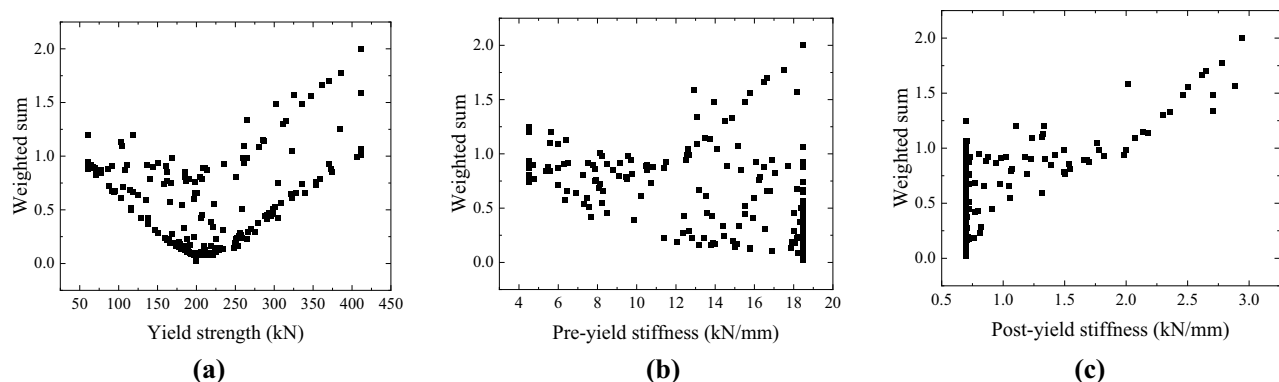


**Fig. 16.** Distribution of iteration particle projections in shear force-displacement weighted optimization space. (a) yield strength direction. (b) pre-yield stiffness direction. (c) post-yield stiffness direction.

bearing Y4Q520 × 135G0.8, the displacement is reduced by 36.6%, confirming a significant optimization effect.

#### *Bearing multi-parameter optimization with a weighted sum of shear force and displacement as the objective function*

In practical seismic design, multiple seismic responses are sometimes considered simultaneously. Therefore, under the James earthquake excitation and using time-history analysis, the improved APSO algorithm is employed with the objective function defined as the weighted sum of pier bottom shear force and pier top displacement to optimize the bearing parameters.

To visually display the distribution of particle parameter combinations within the optimization space, scatter plots of particle projections along various parameter directions are provided (see Fig. 16). It is observed that the yield strength direction exhibits a V-shaped distribution with convergence around 199.7 kN; the pre-yield stiffness direction converges at the maximum value of 18.5 kN/mm; and the post-yield stiffness direction converges at the minimum value of 0.7 kN/mm. To further illustrate the iterative paths and outcomes, the trajectories of 8 randomly selected particles are plotted as line graphs in Fig. 17.

Table 15 shows the optimal parameter combinations achieved using the weighted sum objective function, along with their corresponding optimization rates relative to the original bearing Y4Q520 × 135G0.8.

From Fig. 17; Table 15, it can be concluded that:

- (1) In the yield strength direction, convergence begins around the 9th iteration and is essentially complete by the 15th iteration; in the pre-yield stiffness direction, convergence is reached around the 10th iteration; and in the post-yield stiffness direction, convergence is achieved around the 8th iteration.
- (2) The objective function stabilizes after approximately 10 iterations, with an estimated 50% improvement in convergence speed. When considering both shear force and displacement simultaneously, the optimized parameters reduce the weighted sum objective function value—shear force is reduced by 14.3% at minimum and 43.6% at maximum, and displacement is reduced by 23.8% at minimum and 37.6% at maximum. Relative to the original bearing Y4Q520 × 135G0.8, shear force decreases by 20.7% and displacement by 35.8%, demonstrating a clear and effective optimization.

#### **Optimization results analysis**

Under the excitation of the James earthquake, the nonlinear characteristic parameters of the seismic isolation bearings for the isolation linear continuous girder bridge were optimized using different methods. The optimization results are presented in Table 16; Figs. 18, 19 and 20.

From these results, it can be seen that although the computational burden of the APSO algorithm is greater than that of the orthogonal experiment, the improvement ultimately achieved by the APSO algorithm far exceeds the improvements achieved by the other two optimization methods. In the parametric optimization design for the bridge, the parameter combination derived from the single-parameter sensitivity analysis is highly dependent on the sensitivity of each parameter, which leads to significant variability in the optimization outcomes; although the orthogonal experiment approach requires relatively low effort, its optimization performance is comparatively insufficient. In contrast, the APSO algorithm provides an accurate and optimal parameter combination with the best optimization effect, albeit at the expense of a relatively higher computational workload.

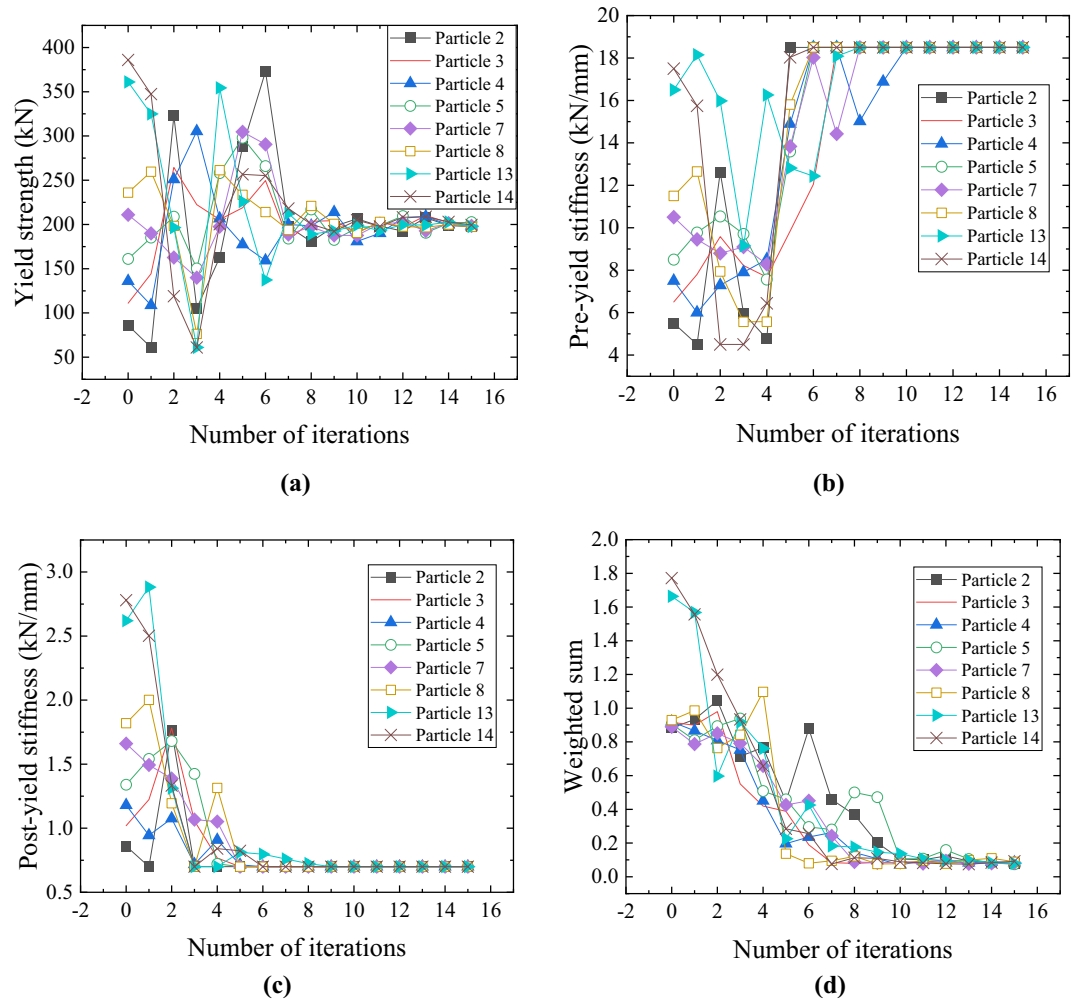


**Fig. 17.** Iteration particle projections along parameter directions in the optimization space. (a) yield strength direction. (b) pre-yield stiffness direction. (c) post-yield stiffness direction. (d) objective function value direction.

Yield strength (kN)	Pre-yield stiffness (kN/mm)	Post-yield stiffness (kN/mm)	Resulting displacement (mm)	Resulting shear force (kN)	Displacement reduction (%)	Shear force reduction (%)
199.7	18.5	0.7	239.73	1383.26	35.8%	20.7%

**Table 15.** The optimal parameter combination and optimization rate of the support.

### Conclusion

This study presents an improved PSO algorithm, termed Adaptive Particle Swarm Optimization (APSO), specifically tailored for the multi-parameter optimization of seismic isolation bearings in continuous girder bridges. By adaptively adjusting inertia and learning factors, as well as refining the search strategy, APSO significantly enhances exploration of the design space. Numerical experiments demonstrate that APSO achieves three clear advancements:

1. APSO reduces the required computational iterations by approximately 40% compared to the standard PSO algorithm, thus markedly shortening optimization time while maintaining or even improving solution accuracy.
2. APSO efficiently handles complex interactions among multiple nonlinear characteristic parameters—including yield strength, pre-yield stiffness, and post-yield stiffness—making it particularly effective for both straight and curved continuous girder bridges. This efficiency ensures reliable convergence to the global optimum even in large-scale optimization scenarios.

Optimization methods	Target function	Parameter combinations				Shear force optimization rate
		Yield strength (kN)	Pre-yield stiffness (kN/mm)	Post-yield stiffness (kN/mm)	Displacement optimization rate	
Single-parameter sensitivity	pier bottom shear force	167.8	9.3	1.4	-	18.27%
		96	17.3	1.4	-	1.36%
		96	9.3	0.7	-	13.68%
	pier top displacement	274.6	9.3	1.4	21.17%	-
		96	18.5	1.4	4.46%	-
		96	9.3	0.7	9.96%	-
	shear force-displacement	167.8	9.3	1.4	14.36%	18.27%
		96	17.3	1.4	3.80%	1.36%
		96	9.6	0.7	9.96%	13.68%
Orthogonal experiment	pier bottom shear force	140	15	1.26	-	10.15%
	pier top displacement	220	15	1.26	26.69%	-
	shear force-displacement	220	15	1.26	10.15%	6.52%
APSO	pier bottom shear force	150	18.5	0.7	-	22.20%
	pier top displacement	210	18.5	0.7	36.60%	-
	shear force-displacement	199.7	18.5	0.7	35.80%	20.70%

**Table 16.** Optimal bearing parameter combinations and optimization rates under different optimization methods.

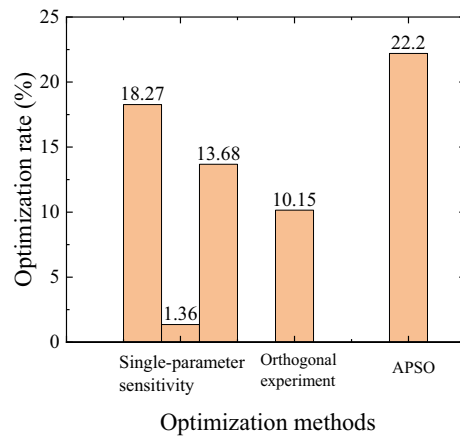


**Fig. 18.** Results of parameter optimization with pier bottom shear force as the target function.

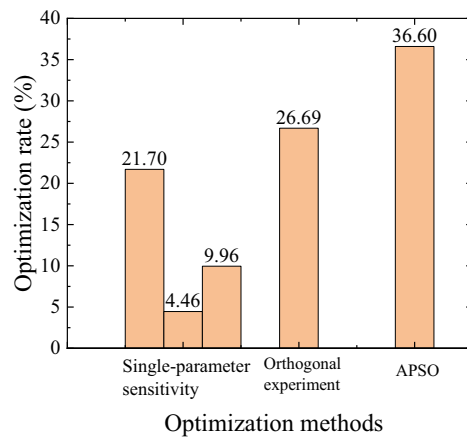


**Fig. 19.** Results of parameter optimization with pier top displacement as the target function.

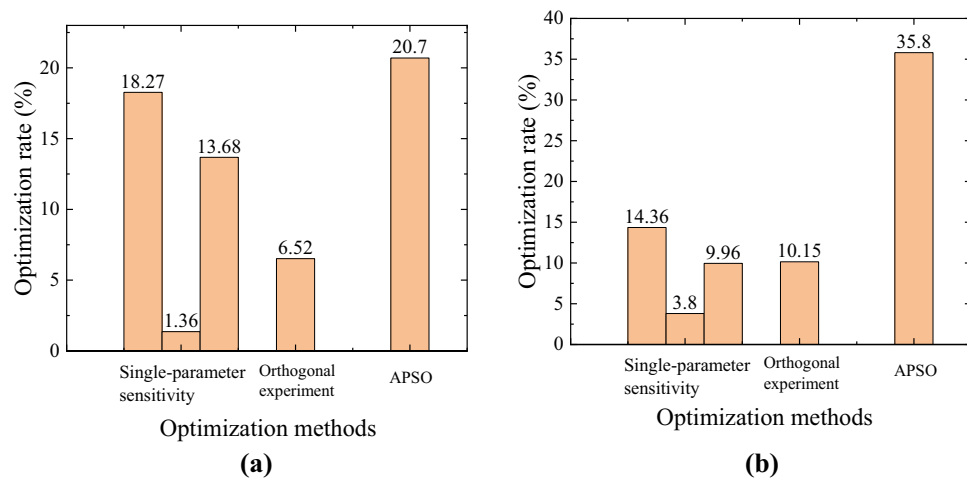


**Fig. 20.** Results of parameter optimization with shear force-displacement weighted sum as the target function. (a) pier bottom shear force. (b) pier top displacement.

3. APSO demonstrates robust scalability and adaptability, providing a practical solution for overcoming computational challenges associated with extensive search domains and intricate parameter dependencies in real-world structural engineering applications.

Despite these advancements, the current study has certain limitations. The proposed APSO algorithm's performance validation relies primarily on numerical simulations; experimental validations with physical models or real-world structures have not yet been conducted. Additionally, the algorithm's performance may vary under significantly different bridge configurations that were not explicitly considered in this study.

Looking ahead, extending APSO to more sophisticated bearing configurations or diverse structural components constitutes a valuable avenue for future research. Furthermore, integrating APSO with advanced modeling frameworks and real-time monitoring technologies may facilitate dynamic adaptive optimization, significantly enhancing seismic resilience and efficiency in bridge design across varying loading conditions.

### Data availability

The data that support the findings of this study are available from the corresponding author upon reasonable request.

Received: 14 February 2025; Accepted: 12 May 2025

Published online: 27 May 2025

### References

1. Elnashai, A. S. & Di Sarno, L. *Fundamentals of Earthquake Engineering: from Source To Fragility* (Wiley, 2015).
2. Xie, H. et al. Preliminary research and scheme design of deep underground in situ geo-information detection experiment for geology in time. *Int. J. Min. Sci. Technol.* **34**, 1 (2024).
3. Castillo, E., Mínguez, R. & Castillo, C. Sensitivity analysis in optimization and reliability problems. *Reliab. Eng. Syst. Safe.* **93**, 1788 (2008).
4. Amiri, G. G., Namiranian, P. & Amiri, M. S. Seismic response of triple friction pendulum bearing under near-fault ground motions. *Int. J. Struct. Stab. Dy.* **16**, 1550021 (2016).
5. Peng, Y., Ma, Y., Huang, T. & De Domenico, D. Reliability-based design optimization of adaptive sliding base isolation system for improving seismic performance of structures. *Reliab. Eng. Syst. Safe.* **205**, 107167 (2021).
6. Zhong, J., Wan, H., Yuan, W., He, M. & Ren, W. Risk-informed sensitivity analysis and optimization of seismic mitigation strategy using Gaussian process surrogate model. *Soil. Dyn. Earthq. Eng.* **138**, 106284 (2020).
7. Gur, S., Mishra, S. K. & Chakraborty, S. Stochastic optimization of shape-memory-alloy rubber bearing (SMARB) for isolating buildings against random earthquake. *Struct. Control Health Monit.* **21**, 1222 (2014).
8. Pang, Y., He, W. & Zhong, J. Risk-based design and optimization of shape memory alloy restrained sliding bearings for highway bridges under near-fault ground motions. *Eng. Struct.* **241**, 112421 (2021).
9. Xia, Z. et al. Model updating of an existing Bridge with high-dimensional variables using modified particle swarm optimization and ambient excitation data. *Measurement* **159**, 107754 (2020).
10. Tran-Ngoc, H. et al. An efficient approach to model updating for a multispan railway Bridge using orthogonal diagonalization combined with improved particle swarm optimization. *J. Sound Vib.* **476**, 115315 (2020).
11. Chen, Z., Cao, H., Ye, K., Zhu, H. & Li, S. Improved particle swarm optimization-based form-finding method for suspension Bridge installation analysis. *J. Comput. Civil Eng.* **29**, 4014047 (2015).
12. Li, J. et al. Optimal sensor placement for long-span cable-stayed Bridge using a novel particle swarm optimization algorithm. *J. Civ. Struct. Health.* **5**, 677 (2015).
13. Quaranta, G., Marano, G. C., Greco, R. & Monti, G. Parametric identification of seismic isolators using differential evolution and particle swarm optimization. *Appl. Soft Comput.* **22**, 458 (2014).
14. Zhang, J. et al. AVA simultaneous inversion of prestack seismic data using particle swarm optimization. *J. Earth Sci-China.* **29**, 1390 (2018).

15. Wei, B. et al. Seismic response prediction and fragility assessment of high-speed railway bridges using machine learning technology. *Structures* **66**, 106845 (2024).
16. Wei, B., Tan, H., Wan, K., Sun, Z. & Li, S. Seismic performance of railway bridges with novel ductile piers under near-fault earthquakes. *Transp. Geotech.* **46**, 101241 (2024).
17. Işık, M. F. et al. A hybrid artificial neural network—Particle swarm optimization algorithm model for the determination of target displacements in mid-rise regular reinforced-concrete buildings. *Sustainability-Basel* **15**, 9715 (2023).
18. Wang, Z. Multi-objective Comprehensive Optimal Management of Construction Projects Based on Particle Algorithm. *Informatika-Lithuan* **43** (2019).
19. Afzal, S., Shokri, A., Ziapour, B. M., Shakibi, H. & Sobhani, B. Building energy consumption prediction and optimization using different neural network-assisted models; comparison of different networks and optimization algorithms. *Eng. Appl. Artif. Intel.* **127**, 107356 (2024).
20. Fang, R. & Popole, Z. Multi-objective optimized scheduling model for hydropower reservoir based on improved particle swarm optimization algorithm. *Environ. Sci. Pollut R.* **27**, 12842 (2020).
21. Lin, Y., Song, Z., Lv, R., Ma, A. & Dong, C. presented at the 2022 34th Chinese Control and Decision Conference (CCDC), (unpublished). (2022).
22. Wei, W. & Yi, Z. presented at the 2019 Chinese Control And Decision Conference (CCDC), (unpublished). (2019).
23. Wolpert, D. H. & Macready, W. G. No free lunch theorems for optimization. *IEEE T Evolut Comput.* **1**, 67 (1997).
24. Shi, Y. & Eberhart, R. presented at the IEEE international conference on evolutionary computation proceedings. IEEE world congress on computational intelligence (Cat. No. 98TH8360), 1998 (unpublished). (1998).
25. Ozdemir, G. & Dicleli, M. Effect of lead core heating on the seismic performance of bridges isolated with LRB in near-fault zones. *Earthq Eng Struct D* **41** (2012). (1989).
26. Mahamied, A., Yasin, A. A., Alzubi, Y., Al Adwan, J. & Mahamied, I. Influence of vertical irregularity on the seismic behavior of base isolated RC structures with lead rubber bearings under Pulse-Like earthquakes. *Health Monit.* **17**, 501 (2023).
27. Wei, B. et al. Decoupled calculation and case study analysis of friction pendulum bearing considering the jumping-off effect. *Int J. Struct. Stab. Dy* **2550195** (2024).
28. MoTotPsRo, C. Lead rubber bearing isolator for highway bridge. (2011).

### Author contributions

Conceptualization, W.Z.; methodology, W.Z.; software, Y.Q.; validation, Y.Q., and Y.B.; data curation, W.Z.; writing—original draft preparation, Y.B.; writing—review and editing, J.S., and T.K.; supervision, W.Z.; project administration, J.S.; funding acquisition, W.Z. All authors have read and agreed to the published version of the manuscript.

### Funding

This research was funded by the Sichuan Natural Science Foundation of China under grant number 2024NS-FSC0171.

### Declarations

### Competing interests

The authors declare no competing interests.

### Additional information

**Correspondence** and requests for materials should be addressed to Z.W.

**Reprints and permissions information** is available at [www.nature.com/reprints](http://www.nature.com/reprints).

**Publisher's note** Springer Nature remains neutral with regard to jurisdictional claims in published maps and institutional affiliations.

**Open Access** This article is licensed under a Creative Commons Attribution-NonCommercial-NoDerivatives 4.0 International License, which permits any non-commercial use, sharing, distribution and reproduction in any medium or format, as long as you give appropriate credit to the original author(s) and the source, provide a link to the Creative Commons licence, and indicate if you modified the licensed material. You do not have permission under this licence to share adapted material derived from this article or parts of it. The images or other third party material in this article are included in the article's Creative Commons licence, unless indicated otherwise in a credit line to the material. If material is not included in the article's Creative Commons licence and your intended use is not permitted by statutory regulation or exceeds the permitted use, you will need to obtain permission directly from the copyright holder. To view a copy of this licence, visit <http://creativecommons.org/licenses/by-nc-nd/4.0/>.

© The Author(s) 2025